Composites Part C: Open Access 3 (2020) 100068

Contents lists available at ScienceDirect

Composites Part C: Open Access

journal homepage: www.elsevier.com/locate/jcomc

3D printing of syntactic foam cored sandwich composite

Dileep Bonthu[a], H.S. Bharath[a], Suhasini Gururaja[b], Pavana Prabhakar[c], Mrityunjay Doddamani[a,*]

[a] Advanced Manufacturing Laboratory, Department of Mechanical Engineering, National Institute of Technology Karnataka, Surathkal 575025, India
[b] Aerospace Engineering, Indian Institute of Science, Bengaluru 560012, India
[c] Department of Civil and Environmental Engineering, University of Wisconsin-Madison, Madison 53706, WI, USA

ARTICLE INFO

Keywords:
FFF
3DP
HDPE
GMB
Sandwich

ABSTRACT

In additive manufacturing, fused filament fabrication (FFF) based three-dimensional printing (3DP) is one of the most popular rapid processing technologies. The key benefit of 3DP is the ability to build integrated, complex, and tailored components. Optimization of feedstock material and associated 3DP process to achieve the required properties for various applications has been an important research field in the recent past. The main objective of this paper is 3DP of syntactic foam cored sandwich composite all at once (skin-core-skin printing in sequence at once). High density polyethylene (HDPE) and glass microballoon (GMB) reinforced (20, 40, and 60 by volume%) HDPE blends are fed into the extruder for manufacturing respective filaments. These HDPE and HDPE/GMB filaments are further sent to the FFF based printer to realize skin and syntactic foam core respectively of the sandwich. The selection of substrate for printing and the crucial issues associated with the printing of core and sandwich composites are analyzed. The present work successfully demonstrates that by optimizing the printing parameters, good quality core and sandwich structures can be printed all at once without any defects. Finally, the suitable printing parameters are used as boundary conditions in finite element (FE) simulation of sandwich for carrying out thermomechanical analysis to analyze the thermal stress distributions in the prints.

1. Introduction

The growth of advanced digital production technology like in additive manufacturing (AM) drives developmental efforts in polymer/polymeric composites processing by providing great flexibility in designing sustainable light-weight construction and multi-functional material systems [1–4]. AM is a layer by layer material addition process to produce 3D objects. FFF based 3DP is one of the most popular AM techniques producing 3D objects by generating a desired printing path through digital slicing of computed designed virtual 3D objects [5,6]. In the FFF process, adhesion of the deposited polymer layers, solidification, and easy removal of prints post-printing are some of the important criteria to obtain defect-free components. Printing multi-material systems at once, like in sandwiches (skin and core), is a challenging task because of differential volumetric shrinkage, adhesion, solidification, and crystallization at the skin-core interface. Commonly used polymers in FFF based 3DP are acrylonitrile butadiene styrene [7,8], polycarbonate [9], polylactide [10], polymethylmethacrylate [11] and HDPE [12,13]. Thermoplastic based polymer composite blends are also being used for printing, enhancing the feedstock material availability based on the specific applications [14–20]. Some of the commonly used fillers used for blend preparation are Al_2O_3 [21], glass [22], iron particles [23], carbon and glass fiber [24]. FFF of propylene/ethylene copolymers and composites reveal that the inclusion of spherical fillers is useful in reducing shrinkage [22,25]. Filler selection is governed by the property requirements and envisaged applications. In recent years, the use of hollow particles like GMB and fly ash cenospheres have increased significantly in the development of low density and high damage tolerant composites [26–31]. Such microballoons are used as fillers in the matrix forming the core and are synthesized earlier by traditional methods wherein higher tooling costs and design constraints raise several challenges in realizing geometrically complex sandwich composites [30,32–35].

Sandwich composite structures are widely explored in the marine, wind, civil, aerospace, and various other fields, due to the several significant advantages over traditional materials, like high specific strength, stiffness, high damping properties, excellent fatigue and corrosion resistance [36–39]. Theories of sandwich structured composites can be traced as early as 1849 CE [40]. However, the ability of sandwich design was realized during World War II. Innovations in the field of aerospace created a demand for light-weight structures with high strength that are highly resistant to damage. Composites with these properties are the first choice for many weight-sensitive applications.

* Corresponding author.
E-mail address: mrdoddamani@nitk.edu.in (M. Doddamani).

https://doi.org/10.1016/j.jcomc.2020.100068
Received 5 October 2020; Received in revised form 28 October 2020; Accepted 29 October 2020

Sandwich composites consist of a thick light-weight slab known as core to which two thin and stiff face sheets are attached, known as skin [41, 42]. The thickness of the core and skin depends on the required properties and specific applications. The selection of materials for sandwich composites depends on loading conditions, cost, quality, constituent materials availability, and functional requirements. Multilayered graphite and carbon epoxy facings are commonly used in aerospace structures, whereas glass epoxy or glass vinyl esters are being used in the frames of civil and marine structures [38]. The design, thickness, and material of core and skin, orientation of material play an essential role in the load-bearing and damping properties of the sandwich structures [43]. The choice of appropriate matrix and filler materials, volume fractions of constituents make them achieve tailored properties. A large number of materials can be used as core based on application and the performance requirements [44]. The commonly used core material can be of low-density solid materials like open and closed cell foams structures, high-density material in cellular form like a honeycomb, high-density material in corrugated form like a truss, etc. The interface between the skin and core is affected by the core structure, which offers additional weightage for designing a sandwich structure according to requirements and operating conditions. The closed cell foam core structure provides superior strength, higher moduli, lower moisture absorption and resistance to flexure, impact and blast in sandwich composites [45–48]. These properties can be tailored based on size, shape, and compositional elements of the pores.

Controlling the pore size and shape in foams is very critical in designing sandwich composites. The need for high strength and stiffness in sandwiches results in two distinct approaches [49] of foams sandwiching between stiffer face-sheets increasing flexural strength [50, 51] and secondly, porosity integration using hollow particles resulting in effective reinforcing effect depending on their wall thickness and volume fraction. These foams filled with hollow particles are called syntactic foams [52–54], which have low moisture absorption, high strength, and better damping property. These foams are multi-functional due to their wide range of mechanical properties, and hence they are used as core material in the sandwich composite for light-weight applications [55–60]. One of the important advantages of these foams is their ability to produce composites with required properties for a specific application. The matrix resin can be selected from the wide range of thermosetting and thermoplastic resins, depending on the operating conditions [61]. Nevertheless, the freedom of sandwich construction is not effectively studied. Still, only a few configurations, such as standard honeycomb [62–64], body-centered cubic lattice [65], pyramidal lattice [66], square honeycomb [67], tetrahedral lattice [68], diamond honeycomb [69], etc. are synthesized using conventional processing routes. Because of the production limitations, traditional production processes for sandwiches are limited for simple geometries [70]. In handling extreme loads upon impact, intricate geometrical sandwich designs are essential. The multistage processing and associated tooling in conventional manufacturing pose challenges in realizing geometrically integrated complex-shaped sandwich composites. The possibility of realizing such an optimized complex light-weight integrated sandwich design using FFF based 3DP is explored in this paper. The focus is on addressing issues related to printing defect free syntactic foam cored sandwich all at once i.e. fabricating sandwich with lower skin-core-upper skin continuously as against separate processing and consolidation of skin and core in conventional manufacturing.

GMBs are widely used in developing light-weight thermoplastic syntactic foams for weight-sensitive structures [71]. Compared to fly ash cenosphere based closed cell foams, GMBs exhibit better mechanical properties due to the defect-free surface and higher sphericity [72,73]. Dimensionally stable prints can be achieved by the stiffer GMB inclusions in HDPE. In the present work, 20, 40, and 60 by volume% GMBs are blended in the HDPE matrix and are subsequently extruded in the filament form. Neat HDPE is also extruded from their pellets using a single screw extruder. These filaments are fed to FFF based 3DP for fabricating syntactic foam cored sandwich at once made of HDPE skin and GMB/HDPE core. Quality of prints mainly depends on parameters like extrusion temperature, nozzle and bed temperature, the orientation of print,% of infill, raster width, and layer height [74]. The selection of substrate material for printing and issues related to the printing and morphology of printed samples are elaborately discussed, and the suitable printing parameters for defect-free syntactic foam cored sandwich are presented. Printing samples with suitable parameters reduces defects (warpage, delamination, porosity) by opt raster diffusion and good bonding at the skin-core interface enhancing the load-bearing capacity. These printing parameters are used in finite element (FE) simulation of syntactic foam cored sandwich composites to investigate thermal stress distribution by performing thermomechanical analysis. Such an analysis helps in understanding the quantum of built-in residual thermal stresses developed during 3DP.

2. Experimental approach

2.1. Materials

Fig. 1a shows a representative image of HDPE (HD50MA180) obtained from IOCL, Mumbai, having an average granule size of ~3 mm. The smooth texture of HDPE is seen in Fig. 1b. Table 1lists the typical characteristics of HDPE granules. GMBs (iM30k) supplied from 3 M (Fig. 1c) are utilized as filler, having 15.3±1.63 μm diameter, density of 0.6 gm/cm^3, and 1.4±0.079 μm wall thickness. Fig. 1d presents a scanning electron microscope (SEM) image of GMBs wherein spherical particles without any surface defects are clearly visible. Such features of GMBs result in uniform resin spread around them, aiding effective load transfer across the interface. These GMBs with varying volume fraction are blended with the HDPE matrix.

2.2. Blend preparation and filament fabrication

Blends of HDPE and GMB are prepared using Brabender (16CME SPL) to develop feedstock foam filaments for 3D printing of sandwich composites. Blending is carried out at an optimized speed of 10 rpm at 160 °C [75] by varying 20, 40, and 60% volume fraction of GMB in HDPE (H). These different volume fractions are denoted as H20, H40, and H60, respectively. HDPE pellets and H20 - H60 blends are dried at 80 °C in the oven for 24 h before gravity feeding into the hopper of the single screw extruder (25SS/MF/26, L/D ratio - 25:1, Aasabi machinery Pvt. Ltd., Bombay). The quality of extruded filament depends on barrel temperature, die temperature, screw speed, and take off unit speed. The suitable barrel and die temperatures convert solid pellets into semi solid-state and extrude it from the die without any material blockage. The filament size depends on the extrusion rate (screw speed and take-off speed). HDPE and foam pellets are fed to the extruder with the temperature profile of 145-150-155-145 °C from the feed to the die section, screw, and take off unit speed of 25 and 11.5 rpm, respectively to produce the filament of 2.85 ± 0.05 mm diameter. All these parameters have been chosen by considering HDPE melting temperature, uniform and homogeneous mixing of GMB in HDPE without breakage, rheological behavior of blends, and presence of porosity, if any, during extru-

Table 1
Typical Characteristics of HDPE granules*.

Property	Typical Value
Melt flow index	20 gm/10 min
Density	0.950 gm/cm^3
Flexural Modulus	750 MPa
Vicat Softening Point	124 °C
Tensile Strength at Yield	22 MPa
Elongation at Yield	12%

* As mentioned by the supplier.

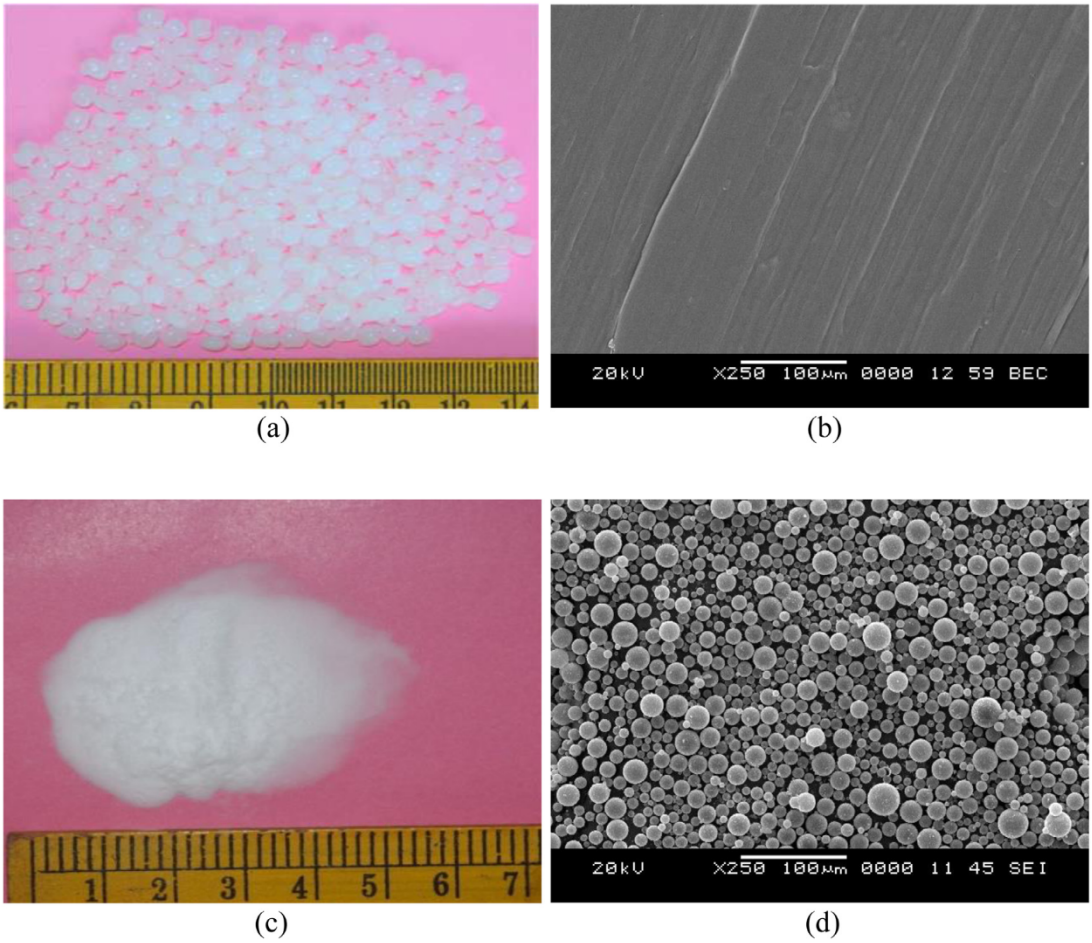

Fig. 1. HDPE (a) granules (b) micrograph; GMB (c) in powder form and (d) SEM image.

sion [76]. With an increase in GMB content, void% increases, and it is in the range of 0.84 to 7.79% for extruded H-H60 filaments [76]. These additional porosities, if transferred to printed samples, form a three-phase syntactic foam, which might enhance damping capabilities. Fig. 2a represents the circular cross-section of extruded H60 filament. H20 filament at higher magnification show uniform dispersion of GMBs in the matrix without any particle breakage (Fig. 2b), confirming the suitability of chosen extrusion parameters. The extruded H60 filament is photographed and presented in Fig. 2c.

2.3. 3D printing of sandwich

The sandwich structure consists of skin (upper and lower) and the core (middle position). The printing parametric optimization is carried for the core first, being thicker (multiple printing layers). The filaments having the composition of H-H60 are fed to FFF based 3D printer (Star, AHA 3D, Jaipur). The filaments are melted in the nozzle (0.5 mm diameter) head of the printer for layered deposition. The 3D printer has two nozzles, namely, primary (N1) and secondary (N2). N1 and N2 are fed with HDPE and foam filaments, respectively. Both nozzles are utilized while printing the sandwich. While printing sandwich, N1 deposits lower skin (1 mm) followed by N2 depositing core (6 mm). Subsequently, once the core deposition is completed, N1 deposits upper skin (1 mm). Sandwich composites are represented by 'S'. Five samples of each SH20, SH40 and, SH60 are printed for checking the consistency of the chosen printing parameters, which implies that the core of these sandwich composites has 20, 40, and 60% by volume fraction of hollow spheres. The tool path (G-code) for printing is generated through Simplify 3D based on the printing parameters. The G-code is the input for the 3D printer for executing layered deposition. Scanning electron microscope (SEM, JSM 6380LA, JEOL, Japan) is used to examine the distribution of GMB particles, layer adhesion, skin and core bonding, delamination of layers and voids in all the printed samples.

2.4. FE simulation using ANSYS

The 3D printing involves complex heat and mass transfer phenomenon that affects the dimensional accuracy of the final part. The thermomechanical FE simulations are carried out using ANSYS 2020 R1 and suitable printing parameters as boundary conditions to visualize the temperature, and thermal stress distributions in 3D printed SH60 sample (post-printing). A 3D steady-state thermal analysis is conducted, and the temperature distribution is used as load input for static-structural analysis. The Hex20 element having an element size of 1 mm, is used in FE simulations. In pre-processing, the properties of skin and core are defined. Table 3 presents the material properties of the SH60 sample used in the FE analysis. The sandwich sample (bottom and top skin each of 1 mm and foam core of 6 mm thick) is modeled having the dimensions of $180 \times 18 \times 8$ mm^3 with a layer thickness of 0.5 mm, totaling 16 layers. Before meshing, sandwich elements (skin-core-skin) are coupled for effective heat transfer. Fig. 3a and Fig. 3b present a sandwich FE model and mesh, respectively. The free mesh is adopted, forming 25,920 elements and 138,799 nodes. The convection boundary conditions are applied as seen in Fig. 3c, and subsequent analysis is carried out for temperature distribution. The obtained temperature data is taken as load data for static-structural analysis to observe the stress distribution in 3D printed samples through FE simulations.

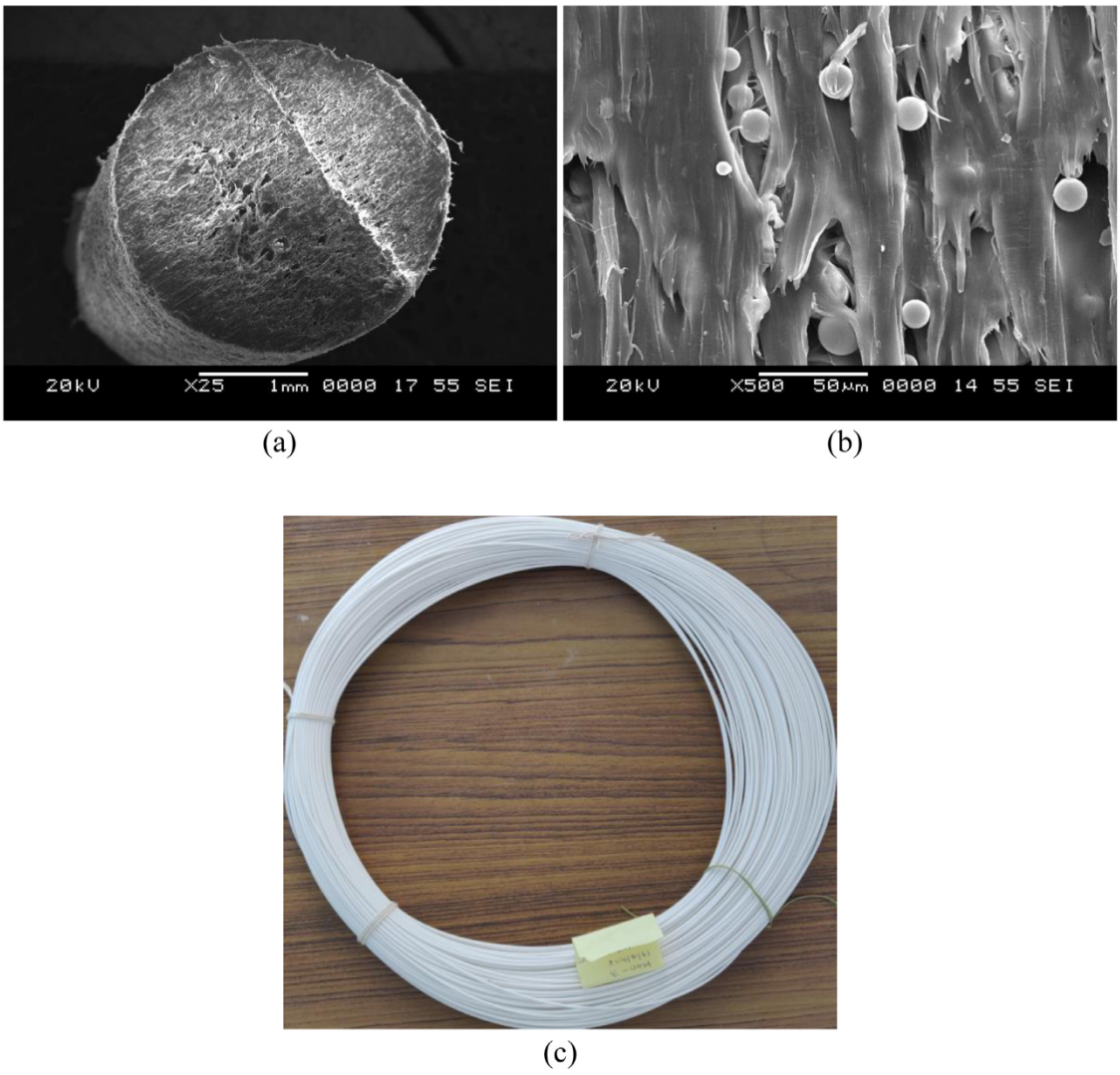

Fig. 2. (a) Micrograph of extruded H60 filament (a) knife cut cross-section of H60 and (c) extruded H60 filament.

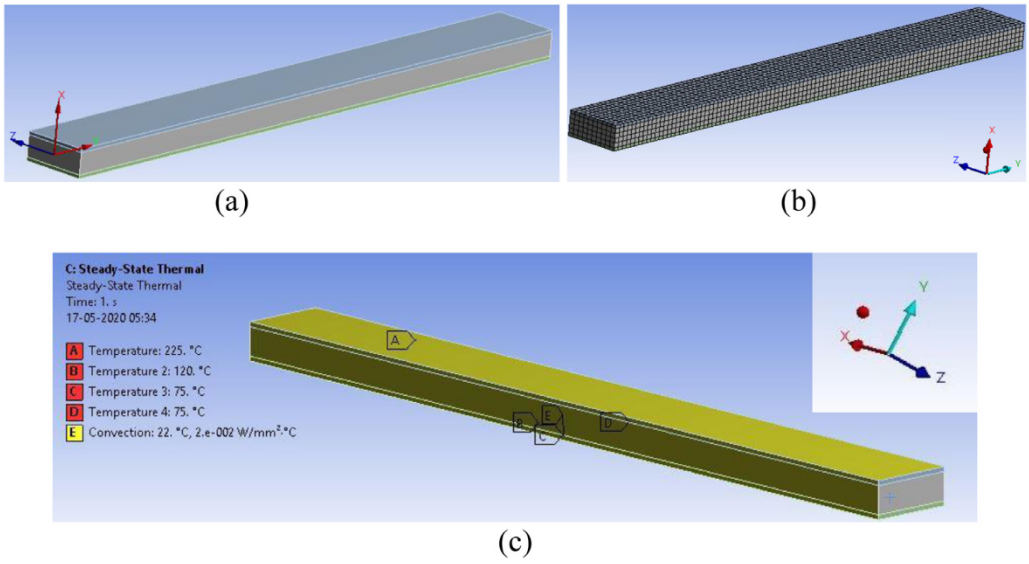

Fig. 3. Sandwich (a) model and (b) mesh and (c) boundary conditions (Table 2) used in FE analysis.

Table 2
Printing parameters used to print core and sandwich structures.

Parameters	H	H20	H40	H60	SH20	SH40	SH60
N1 (°C) - HDPE filament	200–230 *[225]	—–	—–	—–	200–230 **[225]**	200–230 **[225]**	200–230 **[225]**
N2 (°C) - Foam filaments	—–	200–230 **[225]**	230–250 **[245]**	230–250 **[245]**	200–230 **[225]**	230–250 **[245]**	230–250 **[245]**
Extrusion Multiplier	1	1	1	1.2	1	1	1.2
Bed temperature (°C)				80–120 **[120]**			
Chamber temperature (°C)				45–75 **[75]**			
Printing speed (mm/s)				30–40 **[35]**			
Layer thickness (mm)				0.5			
Infill percentage (%)				100			
Raster pattern				Rectilinear			
Raster angle				±45°			

* All the values presented in the square brackets are suitable printing parameters.

Table 3
Material properties used for FE simulation.

SH60	Density (kg/m^3) [76]	CTE (/°C) [76]	Thermal conductivity (Wm^{-1} K^{-1}) [77]	Specific heat (cal/g-K) [77]	Modulus (MPa) [76]	Poisson's ratio
H60	740	8.84×10^{-5}	0.3469	0.3887	1199.26	#0.296
H	950	1.48×10^{-4}	0.4729	0.4617	810.25	0.425 [72]

computed based on rule of mixtures.

Table 4
Evaluation of substrates used for 3DP.

Substrates	Observations
HDPE tape without bed heating (BH)	Good adhesion, Removal difficulty post printing
HDPE tape with BH	Good adhesion, Warped print
Kapton tape without adhesive without BH	Poor adhesion of samples with substrate
Kapton tape with adhesive and BH	Good adhesion, Easily detachable, Warped prints > 6 mm thickness
Kraton™ SEBS FG1901 without BH	Moderate adhesion of samples with substrate.
Kraton™ SEBS FG1901 with BH	Excellent adhesion, Easily detachable without any warpage

3. Results and discussions

3.1. 3D printing

Pilot investigations are carried out to propose the suitable printing parameters for printing core (H20-H60) and sandwiches (SH20-SH60) by exploiting N1 and N2 nozzles available on the commercial FFF based printers. Cores and sandwiches of dimensions $180 \times 18 \times 6$ mm^3 and $180 \times 18 \times 8$ mm^3, respectively, are printed using the parameters as listed in Table 2. GMBs presence in the HDPE matrix reduces the coefficient of thermal expansion leading to lower warpage and samples with dimensionally closer tolerance [76]. Several initial trials in the pilot investigations did not yield high-quality prints. The reasons for such observations and the possible solutions that resulted in sound quality core and sandwiches are discussed hereafter. The suitable parameters (in brackets) are also listed in Table 2 based on the following discussions.

3.1.1. Substrate selection

The selection of a suitable substrate for printing core and sandwich is very crucial from the perspective of adhesion of the raft to the bed and post-print removal without damaging the print. The commercially available printers are fitted with a glass bed that necessitates exploring suitable substrates for layered deposition based on the polymer/polymer composite being considered in this study. The substrate serves two functions: a) Establishes good bonding between the raft and the substrate itself so that the complete part gets built without any defects b) Permits easy removal post-printing without damaging the bottom-most layer of the print. Table 4 presents the evaluation of three substrates (HDPE tape, Kapton tape, and SEBS Kraton™) used in the present work. Initially, samples are printed on HDPE tape without bed heating. The samples showed good adhesion to the substrate but posed difficulty in print pealing from the tape, necessitating subsequent polishing operations. Such post-processing sample polishing routes might add cost, time, lead time, and, most importantly, might pose difficulties for geometrically complex integrated prints. The warpage creeps in when the bed is heated in the presence of HDPE tape as the adhesive effect slowly starts diminishing with increasing bed temperature. As received, Kapton tape did not exhibit any bonding of the print with it. Nevertheless, when it is applied with adhesive, and the bed is heated, good interface bonding and easier removal post-printing is noted. Nonetheless, ends of the prints are warped for the samples having thickness more than 6 mm. This might be due to the higher time lag between the subsequent deposition of layers. With increasing print dimensions (length in the present case), such a time lag increases faster cooling of the earlier layer by the time next layers deposition initiates. Such observation requires a suitable thermoplastic elastomer, which exhibits rubber-like behavior without undergoing vulcanization. Styrene-ethylene-butylene-styrene, also known as SEBS, is one such linear triblock copolymer polymer that is strong and flexible. Kraton™ SEBS FG1901 supplied by RishiChem Distributors Pvt. Ltd., Chennai, is used as the substrate. The printed samples exhibited moderate to excellent adhesion with a substrate based on bed heating conditions and easy detachment post-printing without any warpage. The samples are allowed to cool in the chamber until it achieves the room temperature for minimizing the warpage and residual stresses if any. The Kraton™ SEBS FG1901 substrates are checked for the printing of all the samples (H, H20-H60, SH20-SH60) and observed to be performing very satisfactorily.

3.1.2. Adhesion

The adhesive bonding between the first layer of the print and the substrate depends on the bed and chamber temperature (Table 2). Fig. 4a presents representative print images after peeling the samples from the substrate at different bed and chamber temperatures. The improper adhesion results in non-uniform surface texture in case of 80 °C bed temperature and for chamber temperatures of 45–75 °C (Fig. 4a). Increasing

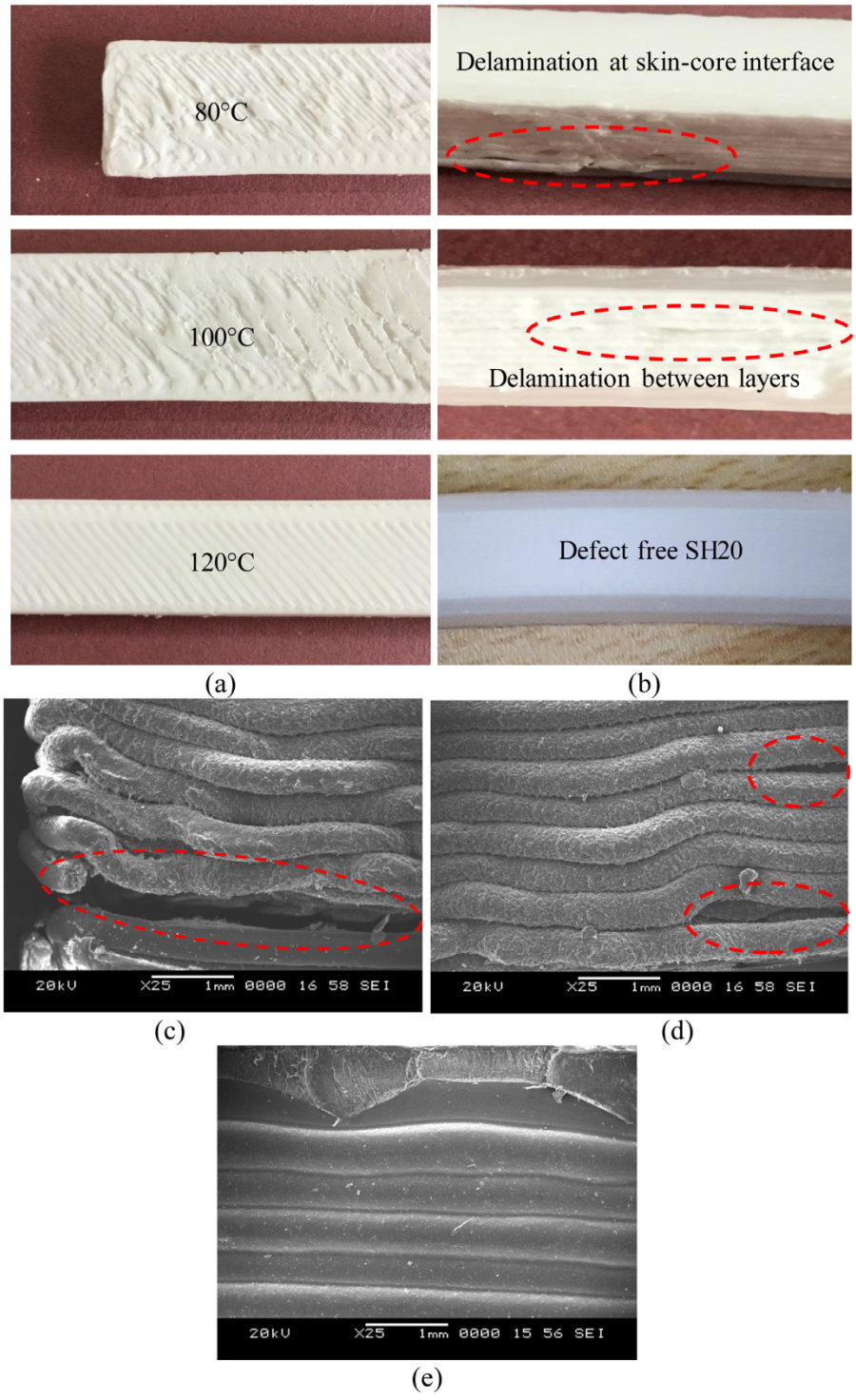

Fig. 4. Representative print images (a) at 80–120 °C bed temperatures with 45–75 °C chamber temperature range (b) of SH20; Micrographs of (c) delamination at skin-core interface (d) delamination within layer and (e) defect free sample.

bed temperature to 100 °C, improper raster diffusion at the base layer forms rough surface and void formations. The perfect bonding, uniform texture, and good quality sample without any defects are observed when the bed and chamber temperatures are maintained at 120 and 75 °C, respectively (Fig. 4a). The uniform and same texture on the bottom and uppermost layers of the printed samples are very crucial to render similar stress state under applied loads. The chamber temperature plays a vital role in controlling delamination at the skin-core interface and within the layers (Fig. 4b). The delamination is significant in the HDPE and their foam prints with larger dimensions due to the higher time lag of printing, resulting in differential cooling rates of the individual layers and higher temperature gradient existing between the layer to be deposited and the earlier laid layer. The appropriate chamber temperature can reduce the temperature gradient between the nozzle, layer, and bed temperatures. As seen from Fig. 4b, below 75 °C chamber temperature, delamination is observed at the skin-core interface and within the layers. The visual observation (Fig. 4b) and the micrographs presented in Fig. 4c and Fig. 4d depict clearly an effect of differential cooling in the form of wavy layers, delamination at the skin-core interface region, and voids within the layers at lower chamber temperatures. The

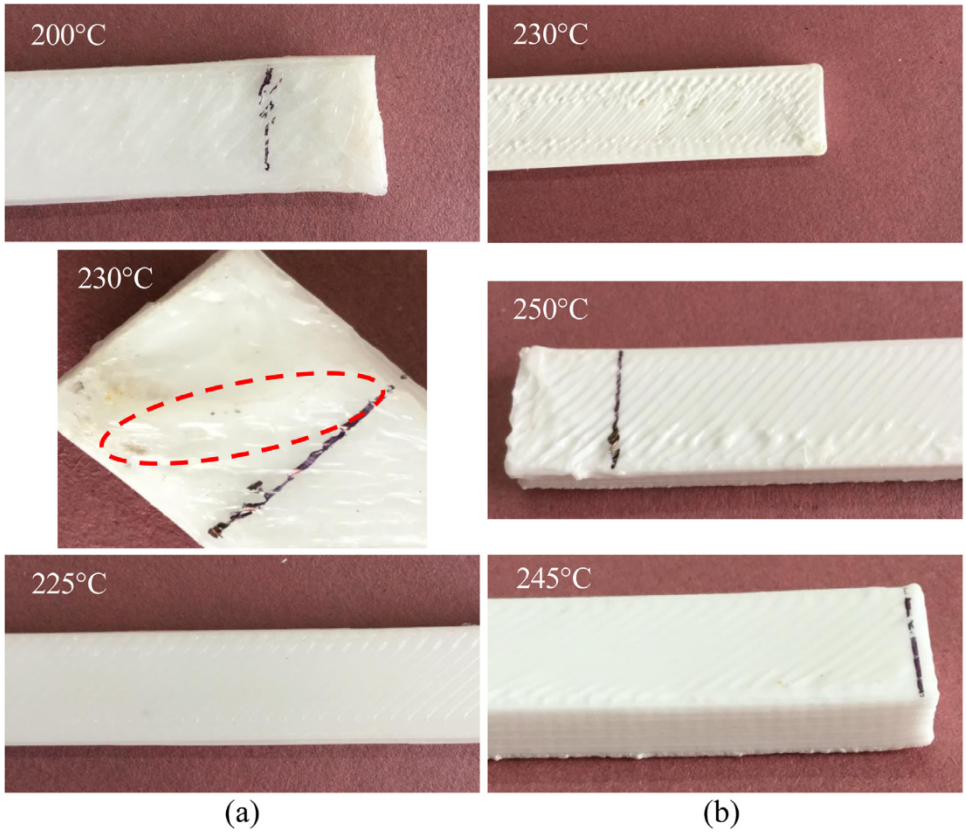

Fig. 5. Prints through (a) N1 and (b) N2.

defect-free sandwich is also presented in Fig. 4b with its micrograph in Fig. 4e. The parallel layers with a seamless interface are clearly visible, signifying the effect of chamber temperature (75 °C) on the printing of multi-material systems, which is a syntactic foam cored sandwich in the present investigation.

3.1.3. Improper flow of material during printing

In printing core and sandwich structures, the flow of material from the nozzle plays a very important role in realizing completely rigid and dense parts. Nozzle (N1 and N2) temperatures and extrusion multiplier are the two parameters that affect the material flow. The temperature of N1 varies from 200 to 230 °C (Table 2) that carries HDPE filament. N1 temperature held at 200 °C results in non-uniform layer deposition, as seen from Fig. 5a. The temperature of 230 °C enables more material flow leading to bulk material deposition at different locations along the sample length. One such location of bulk deposition is marked in Fig. 5a. The material flows smoothly without any difficulty continuously when N1 is set at 225 °C (Fig. 5a). N2 is maintained at 200–230 °C for printing H20. A similar observation is noted as that observed during printing HDPE through N1. Hence N2 is set at 225 °C for printing H20. Fig. 5b presents representative print images of H60 as this composition has maximum GMB content, i.e., the lowest content of HDPE across the chosen compositions. While printing H60, N2 is set initially at 230 °C. As expected, due to lower HDPE content, small pockets (Fig. 5b) are formed at several locations signifying that material did not get deposited. Such an observation might be due to increased viscosity H60 because of a much lower melt flow index (MFI) as compared to H and H20 compositions [76]. Subsequently, to increase the flow of the material, N2 is set at 250 °C. The higher nozzle temperature made the material to flow out continuously but with lumped deposition at several locations. Lowering the N2 temperature by 5 °C (i.e., at 245 °C) resulted in a good print, as seen from Fig. 5b. Similar observations are noted while printing H40 through N2. The extrusion multiplier, as listed in Table 2, is the volume of material flowing out of the nozzles. This parameter decides the raster cross-section, which is dependent on MFI estimations. If the MFI reduction is lower than 60%, the extrusion multiplier is chosen as 1; otherwise, it is set at 1.2 [76].

3.1.4. Prime pillar

The printing of sandwich structures using a single nozzle is a difficult task than printing with two nozzles. This is due to the time lag between the unloading of HDPE filament after skin printing and the loading of foam filaments for core printing. As the time lag increases, the earlier deposited layer solidifies before depositing subsequent layers of the core. Thereby, subsequent layer deposition results in a higher thermal gradient leading to improper layer diffusions, higher residual thermal stresses, a greater amount of shrinkage, and void/pocket formations resulting in defective prints. Further, foam print has to be resumed precisely from the predefined position. There is a good possibility of the nozzle hitting the previously deposited layers. Though this scenario is machine-dependent, isolating such a situation might widen the scope of all the commercially available 3D printers irrespective of their additional features, which comes at a cost. Hence, in the present work, N2 is fed with the foam filament against the printing support structure. Nonetheless, N2 remains idle while N1 is engaged for skin printing leading to improper material flow through N2 when it comes to action. This issue can be resolved by printing a prime pillar (Fig. 6a), which is a small additional print beside the main print. Fig. 6b and Fig. 6c present prints without and with the prime pillar.

3.1.5. Warpage

One of the major problems in 3D printing of HDPE and its foams is the warpage. The bed temperature is one of the important parameters to control the warpage in the printed samples. Other printing parameters are set to suitable values based on the earlier discussions. Fig. 7a presents a representative print image for H60. Similar observations are noted for all the printed cores. At lower bed temperature (80 °C), the

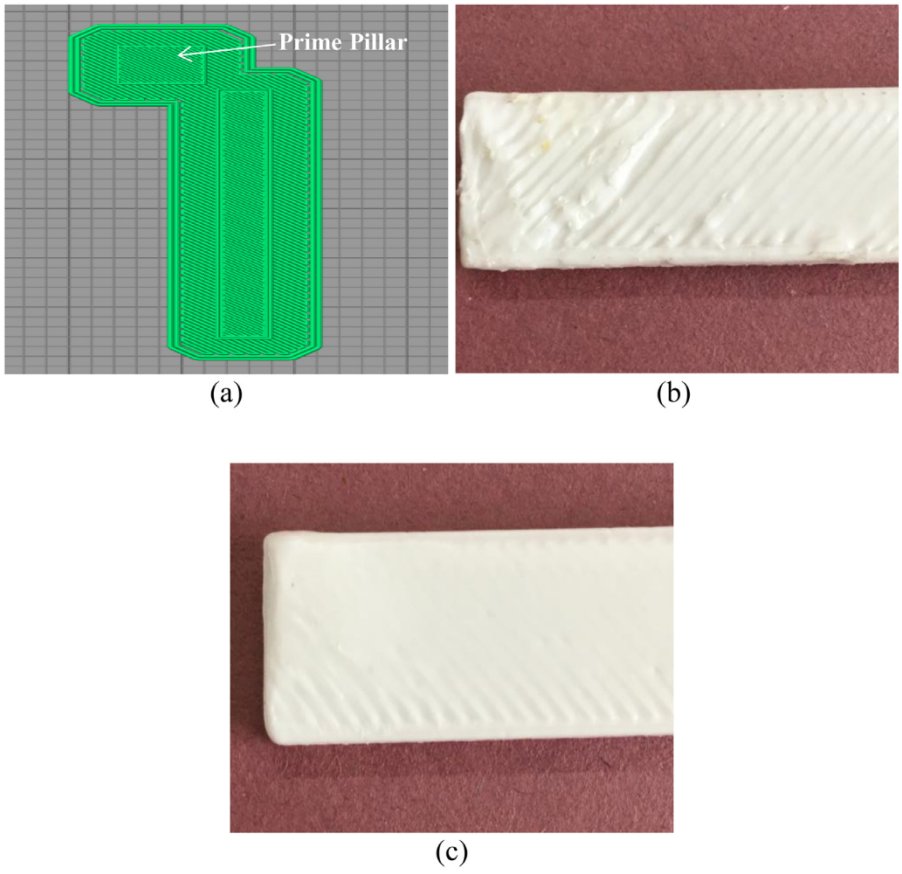

Fig. 6. (a) Schematic representation of the prime pillar, print (a) without and (c) with prime pillar.

post-printing warpage is observed at ends, while at a relatively higher temperature (100 ˚C) its location got shifted at the center lengthwise. At 120 ˚C, H-H60 cores are observed to be printed without any warpage, as seen from Fig. 7a. Nonetheless, in the sandwich, this scenario is expected to change due to HDPE skin and foam core interface. The lower thermal gradient between suitable N1, N2, chamber temperatures, and bed temperature might be the reason for such a defect-free core print. Warpage in the sandwich is observed to be multifold as expected due to different printing temperatures, melt flow index (MFI), and coefficient of thermal expansion (CTE). The print images for the representative SH60 sandwich is presented in Fig. 7b. HDPE shrinks more as compared to GMB/HDPE due to higher MFI and CTE. Though the suitable bed temperature for HDPE printing is 120 ˚C, for sandwich prints, it is varied from 80 to 120 ˚C to analyze warpage magnitude. The warpage magnitude post-printing at the sample ends observed to be 10–20 mm, 2–5 mm in SH20-SH60 at 80 and100 ˚C, respectively. The printing nozzles begin and terminate the printing at the sample ends, which might trigger the warpage at the ends for lower bed temperatures due to a higher thermal gradient between nozzle and bed temperatures. The bed temperature of 120 ˚C is noted to be suitable for sandwich samples (Fig. 7b).

3.1.6. Layer offsetting

Offsetting of the layers is one of the major problems in sandwich printing using multi nozzles. The precise distance between the nozzles which need to be measured periodically influences offset and, in turn, the print quality. The slight change in offset value deteriorates the print, as seen from Fig. 8a. The mechanical elements and the associated errors need to be compensated using the precise measurements between the nozzles, which in turn needs to be set as an offset for N2. Fig. 8a also shows the sample printed with a precisely measured offset value. These offset values play a very crucial role in printing curved sandwich panels and is the future scope of this work.

3.1.7. Printing speed

The surface quality of the prints depends on the printing speed, which is taken in the range of 30–40 mm/s (Table 2) with all the other prevailing printing parameters set at suitable values. The samples printed at 30 mm/s display small islands, as seen from Fig. 8b. This might be due to higher heat concentration at the localized area for a longer time at lower speeds. Higher printing speed (40 mm/s) exhibits voids/pockets due to reduced deposition time. The printing speed of 35 mm/s results in a good smooth surface with a distinct, equally spaced raster. The layer thickness is maintained constant at 0.5 mm to precisely estimate the number of layers to be deposited for an 8 mm thick sandwich in addition to modeling simplicity in thermomechanical analysis using FE simulations. All the core and sandwich configurations are printed at 100% infill, rectilinear pattern, and $\pm 45^{\circ}$ raster angle with two outer perimeter lines and a raft offset of 50 mm. The suitable printing parameters for skin (H), core (H20-H60) and, sandwich composites (SH20-SH60) are represented in Table 2.

3.1.8. Micrographic investigations

The freeze fractured micrographic investigations are carried out on syntactic cored sandwich composites printed using the lowest (Fig. 9a) and suitable values (Fig. 9b), as listed in Table 2. The effect of improper adhesion and inadequate material flow due to the lower nozzle, bed, and chamber temperature is clearly visible in Fig. 9a. The voids in the skin and skin-core interface are due to localized diffusion between the raster amid 100% infill. Nonetheless, such a structure resembles two and three-phase skin and syntactic foams, respectively, that might enhance energy absorbing capabilities at the expense of the required strength. Fig. 9b exhibits a seamless interface between the skin-core-skin interface without any voids and defects, as discussed earlier. FFF based 3D printing is typically comprised of two thermal cycles, one during filament extrusion and the other when the material is flowing through printer

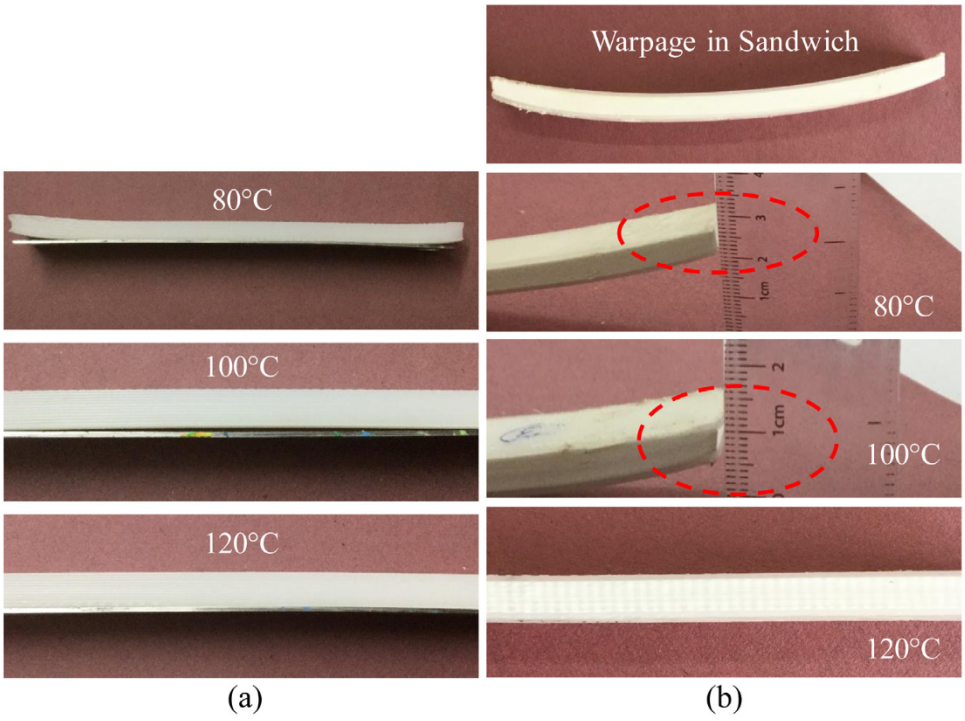

Fig. 7. Warpage in representative (a) H60 (core) and (b) SH60.

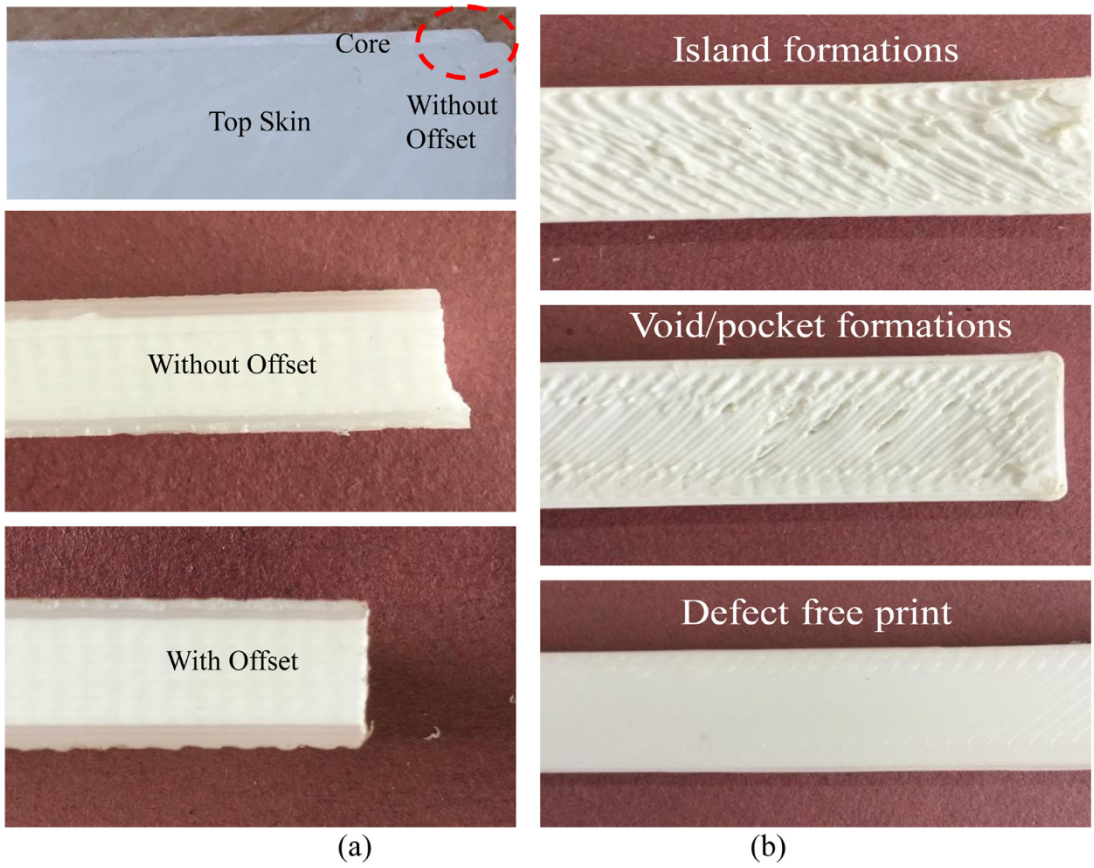

Fig. 8. Representative sandwich prints for effect (a) of layer offset and (b) print speed.

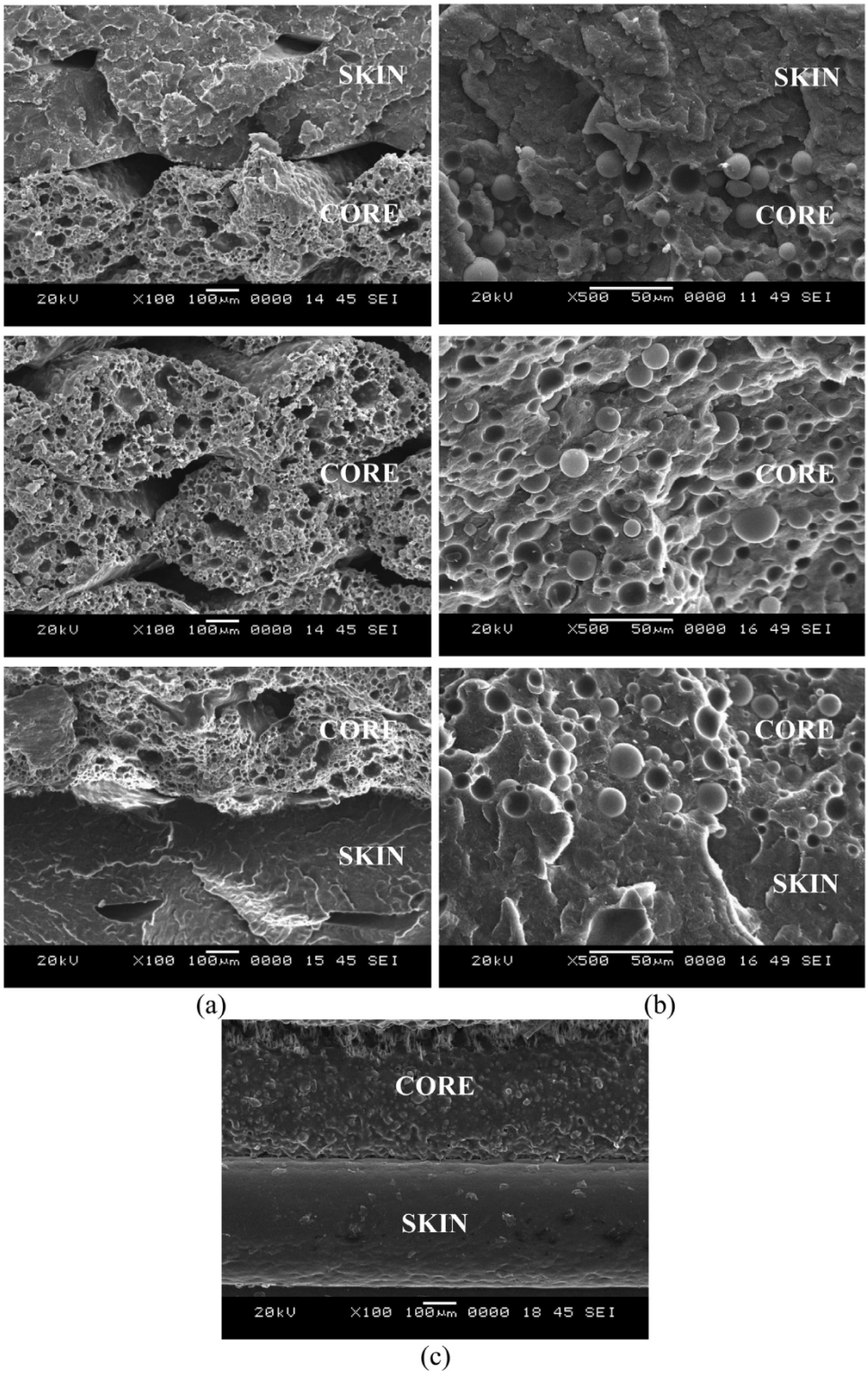

Fig. 9. Freeze fractured micrographs of representative 3DP sandwich (a) using lower and (b) suitable printing parameters from Table 2. (c) Micrograph of the sandwich along thickness.

nozzles for layered deposition. Though authors could successfully print a syntactic foam cored sandwich at once, estimation of thermal stresses is essential for achieving thermal equilibrium faster by reducing the heat gradients across the nozzle, bed, and chamber temperatures during and post-printing. The warpage in the sandwich is substantial as compared to the core, as seen from Fig. 7. The sandwich exhibits warpage post-printing without any delamination between the skin and core (Fig. 7b), signifying the non-uniform thermal stresses. Nonetheless, suitable printing parameters resulted in the sandwich without any warpage, as seen from Fig. 7b. By knowing the temperature distribution in the sound quality sandwich post-printing, particularly across the skin-core interface, localized heating/cooling mechanisms can be deployed to reduce the residual thermal stresses further, which might lead to a sandwich with much better mechanical properties. Thereby, in the present work,

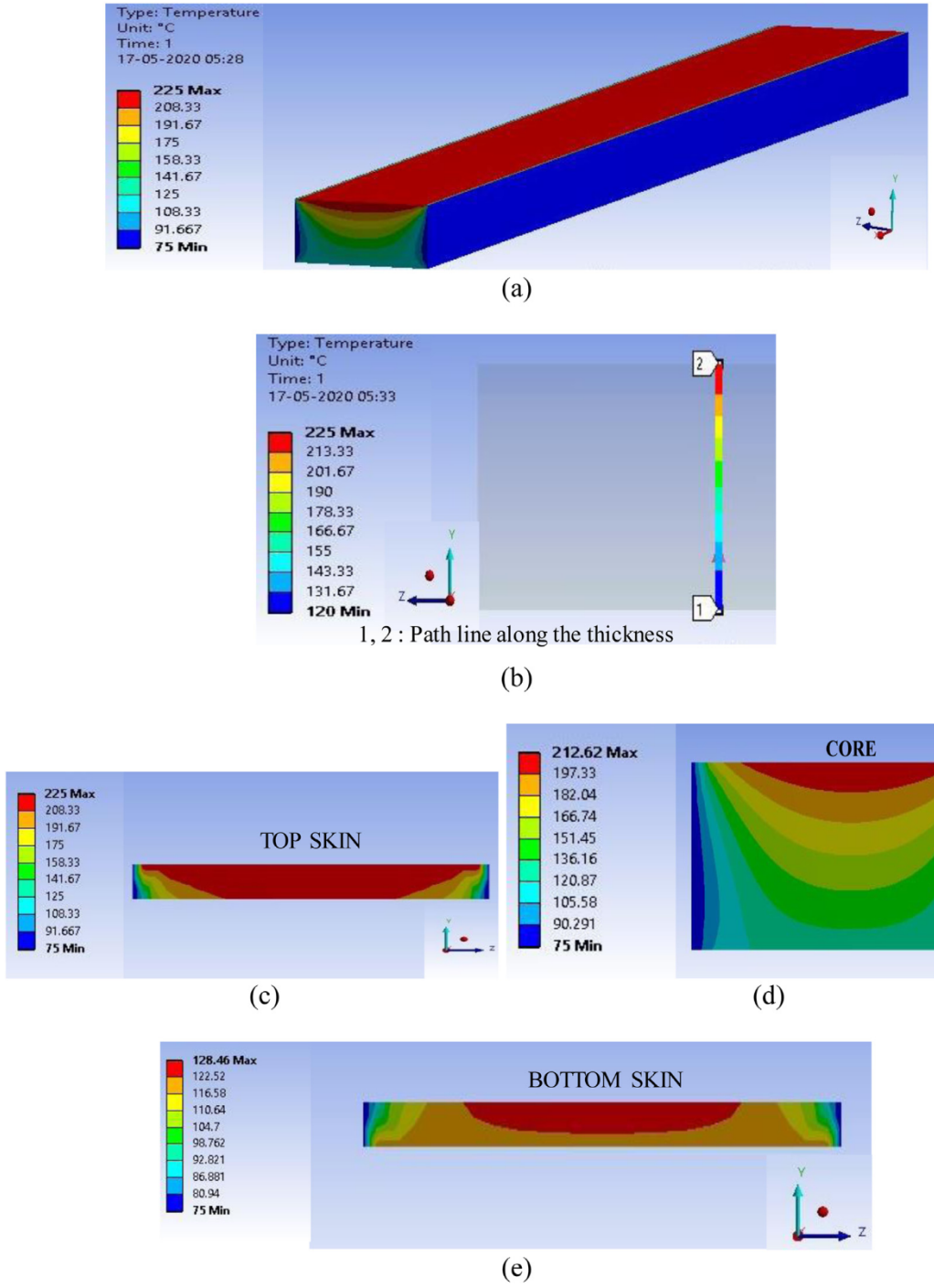

Fig. 10. Temperature distribution in (a) sandwich (b) thickness direction (c) top skin (d) core and (e) bottom skin.

FE simulation of SH60 is adopted to estimate the temperature distribution and thermal stresses using suitable printing parameters, as listed in Table 2.

3.2. Thermomechanical analysis

The results of thermal analysis in the form of temperature distribution are presented in Fig. 10. It is observed that temperature distribution varies from skin to core since convective heat transfer boundary condition is applied wherein chamber temperature is set at 75 °C. The bottom skin is going to have a temperature slightly more than the bed temperature (120 °C). The top layer of the skin is subjected to 225 °C. The sequential deposition of the material is observed clearly in the thermal analysis. Cyclic cooling and heating of the extruded material can be seen as temperature distribution is minimum at the bottom and maximum at the top layer. As the heat gets conducted between layers, the bottom layers were cooled and heated cyclically. The highest temperature is noted to be for the just-deposited layer, whereas the side faces of the sandwich are cooling at a faster rate due to convection. The temperature distribution along the thickness of the sample is presented in Fig. 10b. The temperature distribution of the 3D printed samples mainly depends on the heat transfer coefficient of the surrounding air, nozzle, bed and chamber temperature. By considering all these parameters as boundary conditions, a steady-state thermal analysis is carried out on the SH60.

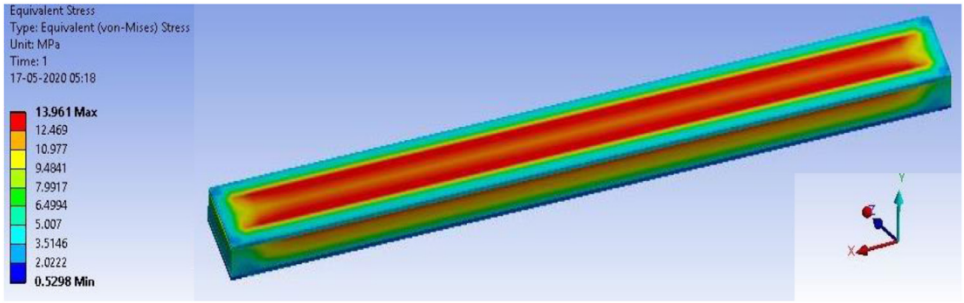

(a)

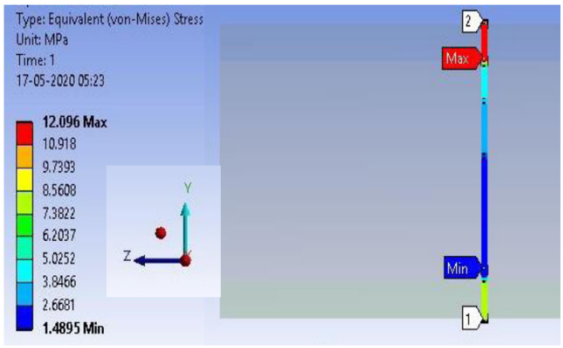

(b)

Fig. 11. Stress (MPa) distribution in (a) SH60 (b) along the thickness.

The temperature variation is observed along with the thickness and in the radial direction. The variation of temperature in the radial direction is due to convective heat transfer at lateral edges resulting in it to be at a lower temperature (75 °C) as compared to the top skin, bottom skin, and at the skin-core interface. The bottom skin is in contact with the printer bed, which is maintained at 120 °C during printing. Due to a sudden decrease in the thermal conductivity at the skin-core interface, the stagnation effect raises the temperature at the top layer (128.46 °C) of the bottom skin (Fig. 10e) and interface as compared to the first layer of the bottom skin. The hollow GMB particles used as filler in the core have lower thermal conductivity increasing conductive resistance (Fig. 10d). The maximum temperature is observed at the top skin (Fig. 10c), which is printed last at 225 °C.

The thermal analysis results of SH60 is imported as the load data for analyzing the thermal stress distribution. Similar boundary conditions are imported from the thermal analysis for structural analysis in addition to the frictionless support for the bottom surface. It is observed that stresses are found to be maximum in the top skin near to the lateral surfaces and minimum at the core (Fig. 11a). Post analysis, stresses at the width and lengthwise center are presented in Fig. 11b and are tabulated in Table 5. The temperature and stress distribution along the thickness of the sandwich are presented in Fig. 12a and Fig. 12b, respectively. Fig. 12a depicts the temperature distribution through the thickness of SH60. As seen from this plot, temperature increases from the bottom to top skin through the foam core. The bottom and top skins proximity, respectively towards bed and nozzle, is the reason for such an observation. The thermal stresses in the top and bottom skin are more as compared to the core section (Fig. 12b) due to the respective thermal properties of skin and core in addition to the resistance offered by the hollow GMB filler particles towards the rate of heat transfer. The stress in the bottom skin is dependent on the bed temperature. The higher thermal stresses in top and bottom skin as compared to the core is due to the associated temperature difference with the direct contact regions. Neat HDPE printed as a bottom skin is in contact with printer bed maintained at 120 °C while top skin is in contact with the ambient chamber. The higher the temperature difference, the higher will the thermal stresses. Further, printed HDPE has a comparatively higher coefficient of thermal expansion (CTE) than the core. Due to a change in the thermal expansion values at the skin-core interface, a sudden drop of thermal stress is observed. The GMB filler particles in the core are less thermally conductive. Due to the different CTE values at the interface of the core and top skin, the drag phenomenon creeps in, resulting in rising of thermal stresses. The stress distribution in the core is designated in four (I – IV) zones. The stress at the bottom skin-core interface suddenly changes the trend and starts decreasing sharply, as seen from zone I in Fig. 12b. The decline continues up to 0.5 mm from the skin-core interface towards the core. This might be due to differential thermal properties of skin and core in addition to the lower thermal conductivity of H60 as compared to H. The stress levels in zone II and III increases from 1.32 to 4.29 MPa. This substantially lowers stress values in the core (zone II and III) is due to hollow GMB particles, which effectively resist the heat transfer because of hollow space within the microspheres. The thermal conduction mode is predominant in neat HDPE, i.e., skin in the present case. The heat transfer mechanism in the GMB/HDPE core is influenced by (i) conduction between HDPE and GMB (ii) convention between the gas molecules present within the hollow space of GMBs [56]. As the GMB content in the HDPE matrix increases, higher resistance to heat flow substantially reduces the thermal stresses developed in the foamed cores as compared to the skins. The rate of thermal stress rise in III is slightly higher than II. Such a marginal change in the slope of III as compared to II might be due to zone III's proximity towards top skin, which is printed at 225 °C. The sudden rise in stress level is observed in zone IV, as it is closer to the top skin.

The FE simulations help in visualizing the stresses at the critical locations. In the present investigations, such locations are at the skin core interface wherein drastic stress level changes are noted though the simulations are carried out at suitable printing parameters. Though the simulation did not show any warpage as expected due to suitable printing parameters, stress levels within the core can be minimized further for achieving thermal equilibrium in the foam cores. The possible strategies could be a) reducing the infill% b) usage of three-phase syntactic foams c) adopting localized cooling. The thermal stress levels in the skin can

Table 5
Temperature and stress distribution along the sandwich thickness computed from FEA.

Region	Sample thickness (mm)	Temperature distribution (°C)	Stress distribution (MPa)
Top Skin	8.0	225	11.54
	7.5	218.91	11.77
	7.0	212.86	12.01
Core	6.5	204.47	4.29
	6.0	196.47	3.90
	5.5	188.63	3.52
	5.0	181.02	3.13
	4.5	173.65	2.75
	4.0	166.53	2.37
	3.5	159.67	2.11
	3.0	153.06	1.86
	2.5	146.68	1.64
	2.0	140.51	1.45
	1.5	134.5	1.32
Bottom Skin	1.0	128.46	7.87
	0.5	124.21	7.89
	0.0	120	7.93

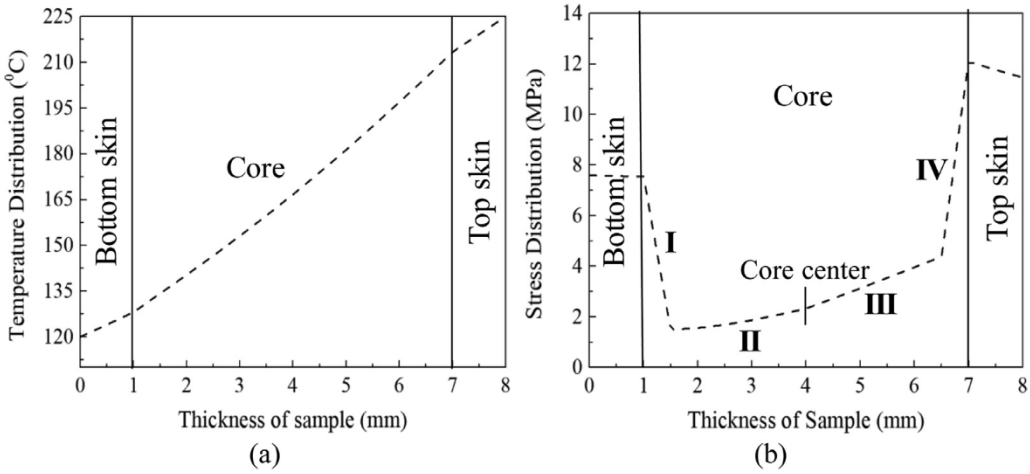

Fig. 12. (a) Temperature and (b) stress distribution along the sandwich thickness post printing.

also be lowered by inducing voids (air/gas entrapment or raster gaps) and lowering the infill%. Nevertheless, the mentioned approaches might compromise strength amid higher damping properties. These strategies can be used based on the envisaged applications.

4. Conclusions

The syntactic foam cores sandwich is successfully 3D printed all at once without any defects. Among many substrates used in commercially available 3D printers for printing, SEBS FG1901 is found to the most suitable for printing the GMB/HDPE cored sandwich. It showed very good adhesion and exhibited easily detachable feature post-printing. Both the nozzles available in printers are utilized for printing sandwich skin and core at once. All the printing parameters are suitable for printing SH20 – SH60 sandwich composites and are listed below:

- Nozzle 1 (N1): 225 °C; Nozzle 2 (N2): SH20 - 225 °C, SH40 and SH60 - 245 °C
- Extrusion Multiplier: SH20 and SH40 - 1, SH60 - 1.2.
- Bed and chamber temperatures of 120 and 75 °C, respectively.
- Speed of printing: 35 mm/s.

The micrographs of printed syntactic foam cored sandwich exhibit the seamless, defect-free interface between the skin and core and within the core layers. The thermomechanical analysis for SH60 is carried out through FE simulations using suitable printing parameters to analyze the temperature and thermal stress distributions. The thermal stress distribution across the sandwich is presented, and the possible strategies for minimizing them is also proposed. Sandwiches printed at once using the proposed methodology, as presented in this paper, avoids the need for adhesive/glue (absence of parent material) used in conventional manufacturing of sandwich composites for assembling core and skin. The enhancement in strength is expected for these sandwich composites, which will be explored in the authors' subsequent efforts.

Acknowledgment

Govt. of India is acknowledged by the authors for funding through SPARC/2018-2019/P439/SL grant for carrying out the research presented here. ME department of NITK is thanked for providing the support and facilities. The support by U.S. ONR-YIP award (Grant no.: N00014-19–1-2206) is acknowledged by the authors.

Data availability

The raw/processed data required to reproduce these findings cannot be shared at this time as the data also forms part of an ongoing study.

References

[1] T.D. Ngo, A. Kashani, G. Imbalzano, K.T.Q. Nguyen, D. Hui, Additive manufacturing (3D printing): a review of materials, methods, applications and challenges, Compos. Part B: Eng. 143 (2018) 172–196.

[2] S. Singh, S. Ramakrishna, R. Singh, Material issues in additive manufacturing: a review, J. Manuf. Process. 25 (2017) 185–200.
[3] J.W. Stansbury, M.J. Idacavage, 3D printing with polymers: challenges among expanding options and opportunities, Dent. Mater. 32 (1) (2016) 54–64.
[4] S.A.M. Tofail, E.P. Koumoulos, A. Bandyopadhyay, S. Bose, L. O'Donoghue, C. Charitidis, Additive manufacturing: scientific and technological challenges, market uptake and opportunities, Mater. Today 21 (1) (2018) 22–37.
[5] N.T. Brian, R. Strong, A.G. Scott, A review of melt extrusion additive manufacturing processes: I. Process design and modeling, Rapid Prototyp. J. 20 (3) (2014) 192–204.
[6] N. Turner Brian, A.Gold Scott, A review of melt extrusion additive manufacturing processes: II. Materials, dimensional accuracy, and surface roughness, Rapid Prototyp. J. 21 (3) (2015) 250–261.
[7] B.M. Tymrak, M. Kreiger, J.M. Pearce, Mechanical properties of components fabricated with open-source 3-D printers under realistic environmental conditions, Mater. Des. 58 (2014) 242–246.
[8] S. Dul, Fused deposition modelling with ABS–graphene nanocomposites Part A Applied science and manufacturing, Composites 85 (2016) 181–191 v.-2016 v.85.
[9] M. Domingo-Espin, J.M. Puigoriol-Forcada, A.-.A. Garcia-Granada, J. Llumà, S. Borros, G. Reyes, Mechanical property characterization and simulation of fused deposition modeling Polycarbonate parts, Mater. Des. 83 (2015) 670–677.
[10] M. Spoerk, F. Arbeiter, H. Cajner, J. Sapkota, C. Holzer, Parametric optimization of intra- and inter-layer strengths in parts produced by extrusion-based additive manufacturing of poly(lactic acid), J. Appl. Polym. Sci. 134 (41) (2017) 45401.
[11] D. Espalin, K. Arcaute, D. Rodriguez, F. Medina, M. Posner, R. Wicker, Fused deposition modeling of patient-specific polymethylmethacrylate implants, Rapid Prototyp. J. 16 (3) (2010) 164–173.
[12] M. Doddamani, Dynamic mechanical analysis of 3D printed eco-friendly lightweight composite, Compos. Commun. 19 (2020) 177–181.
[13] Gupta, N. and M. Doddamani, 3D printing of syntactic foams for marine applications, in Advances in Thick Section Composite and Sandwich Structures: an Anthology of ONR-sponsored Research, S.W. Lee, Editor. 2020, Springer International Publishing: Cham. p. 407–438.
[14] P. Beesetty, A. kale, B. Patil, M. Doddamani, Mechanical behavior of additively manufactured nanoclay/HDPE nanocomposites, Compos. Struct. 247 (2020) 112442.
[15] P. Jeyachandran, S. Bontha, S. Bodhak, V.K. Balla, B. Kundu, M. Doddamani, Mechanical behaviour of additively manufactured bioactive glass/high density polyethylene composites, J. Mech. Behav. Biomed. Mater. 108 (2020) 103830.
[16] B. Patil, B.R. Bharath Kumar, M. Doddamani, Compressive behavior of fly ash based 3D printed syntactic foam composite, Mater. Lett. 254 (2019) 246–249.
[17] B. Patil, B.R. Bharath Kumar, S. Bontha, V.K. Balla, S. Powar, V. Hemanth Kumar, S.N. Suresha, M. Doddamani, Eco-friendly lightweight filament synthesis and mechanical characterization of additively manufactured closed cell foams, Compos. Sci. Technol. 183 (2019) 107816.
[18] A.K. Singh, A.J. Deptula, R. Anawal, M. Doddamani, N. Gupta, Additive manufacturing of three-phase syntactic foams containing glass microballoons and air pores, JOM 71 (4) (2019) 1520–1527.
[19] A.K. Singh, B. Patil, N. Hoffmann, B. Saltonstall, M. Doddamani, N. Gupta, Additive manufacturing of syntactic foams: part 1: development, properties, and recycling potential of filaments, JOM 70 (3) (2018) 303–309.
[20] A.K. Singh, B. Saltonstall, B. Patil, N. Hoffmann, M. Doddamani, N. Gupta, Additive manufacturing of syntactic foams: part 2: specimen printing and mechanical property characterization, JOM 70 (3) (2018) 310–314.
[21] R. Singh, S. Singh, F. Fraternali, Development of in-house composite wire based feed stock filaments of fused deposition modelling for wear-resistant materials and structures, Compos. Part B: Eng. 98 (2016) 244–249.
[22] M. Spoerk, F. Arbeiter, I. Raguž, G. Weingrill, T. Fischinger, G. Traxler, S. Schuschnigg, L. Cardon, C. Holzer, Polypropylene filled with glass spheres in extrusion-based additive manufacturing: effect of filler size and printing chamber temperature, Macromol. Mater. Eng. 303 (7) (2018) 1800179.
[23] S.H. Masood, W.Q. Song, Development of new metal/polymer materials for rapid tooling using fused deposition modelling, Mater. Des. 25 (7) (2004) 587–594.
[24] B. Brenken, E. Barocio, A. Favaloro, V. Kunc, R.B. Pipes, Fused filament fabrication of fiber-reinforced polymers: a review, Addit. Manuf. 21 (2018) 1–16.
[25] M. Spoerk, C. Savandaiah, F. Arbeiter, J. Sapkota, C. Holzer, Optimization of mechanical properties of glass-spheres-filled polypropylene composites for extrusion-based additive manufacturing, Polym. Compos. 40 (2) (2019) 638–651.
[26] M. Doddamani, Influence of microballoon wall thickness on dynamic mechanical analysis of closed cell foams, Mater. Res. Express 6 (12) (2020) 125348.
[27] M. Doddamani, Wear behavior of glass microballoon based closed cell foam, Mater. Res. Express 6 (11) (2019) 115314.
[28] K. Shahapurkar, M. Doddamani, G.C. Mohan Kumar, N. Gupta, Effect of cenosphere filler surface treatment on the erosion behavior of epoxy matrix syntactic foams, Polym. Compos. 40 (6) (2019) 2109–2118.
[29] H.S. Ashrith, M. Doddamani, V. Gaitonde, Effect of wall thickness and cutting parameters on drilling of glass microballoon/epoxy syntactic foam composites, Compos. Struct. 211 (2019) 318–336.
[30] K. Shahapurkar, V.B. Chavan, M. Doddamani, G.C.M. Kumar, Influence of surface modification on wear behavior of fly ash cenosphere/epoxy syntactic foam, Wear 414-415 (2018) 327–340.
[31] C.D. Garcia, K. Shahapurkar, M. Doddamani, G.C.M. Kumar, P. Prabhakar, Effect of arctic environment on flexural behavior of fly ash cenosphere reinforced epoxy syntactic foams, Compos. Part B: Eng. 151 (2018) 265–273.
[32] F.A. Shutov, Syntactic polymer foams, Chromatography/Foams/Copolymers, Springer, Berlin, Heidelberg, 1986.
[33] M.V. Deepthi, M. Sharma, R.R.N. Sailaja, P. Anantha, P. Sampathkumaran, S. Seetharamu, Mechanical and thermal characteristics of high density polyethylene–fly ash Cenospheres composites, Mater. Des. 31 (4) (2010) 2051–2060.
[34] S.N. Patankar, Y.A. Kranov, Hollow glass microsphere HDPE composites for low energy sustainability, Mater. Sci. Eng.: A 527 (6) (2010) 1361–1366.
[35] S.N. Patankar, A. Das, Y.A. Kranov, Interface engineering via compatibilization in HDPE composite reinforced with sodium borosilicate hollow glass microspheres, Compos. Part A 40 (6) (2009) 897–903.
[36] O.T. Thomsen, Sandwich materials for wind turbine blades — present and future, J. Sandw. Struct. Mater. 11 (1) (2009) 7–26.
[37] M. Mohamed, S. Anandan, Z. Huo, V. Birman, J. Volz, K. Chandrashekhara, Manufacturing and characterization of polyurethane based sandwich composite structures, Compos. Struct. 123 (2015) 169–179.
[38] V. Birman, G.A. Kardomateas, Review of current trends in research and applications of sandwich structures, Compos. Part B: Eng. 142 (2018) 221–240.
[39] M. Elamin, B. Li, K.T. Tan, Impact damage of composite sandwich structures in arctic condition, Compos. Struct. 192 (2018) 422–433.
[40] A.K. Noor, W.S. Burton, C.W. Bert, Computational models for sandwich panels and shells, Appl. Mech. Rev. 49 (3) (1996) 155–199.
[41] N. Gupta, S.E. Zeltmann, D.D. Luong, M. Doddamani, 7—Core materials for marine sandwich structures, Mar. Compos.: Des. Perform. (2018) 187. Marine Composites, 1st Edition, Design and Performance, Paperback ISBN: 9780081022641, eBook ISBN: 978008101913.
[42] N. Gupta, S.E. Zeltmann, D.D. Luong, M. Doddamani, et al., Testing of foams, in: S. Schmauder, et al. (Eds.), Handbook of Mechanics of Materials, Springer, Singapore, 2018, pp. 1–40. Editors.
[43] C. Yuan, O. Bergsma, S. Koussios, L. Zu, A. Beukers, Optimization of sandwich composites fuselages under flight loads, Appl. Compos. Mater. 19 (1) (2012) 47–64.
[44] J.R. Vinson, The Behavior of Sandwich Structures of Isotropic and Composite Materials, CRC Press, 1999.
[45] J. Zhang, Q. Qin, C. Xiang, T.J. Wang, Dynamic response of slender multilayer sandwich beams with metal foam cores subjected to low-velocity impact, Compos. Struct. 153 (2016) 614–623.
[46] J. Zhang, Q. Qin, W. Ai, H. Li, T.J. Wang, The failure behavior of geometrically asymmetric metal foam core sandwich beams under three-point bending, J. Appl. Mech. 81 (7) (2014).
[47] J. Zhang, R. Zhou, M. Wang, Q. Qin, Y. Ye, T.J. Wang, Dynamic response of double-layer rectangular sandwich plates with metal foam cores subjected to blast loading, Int. J. Impact Eng. 122 (2018) 265–275.
[48] M.R. Doddamani, S.M. Kulkarni, Kishore, Behavior of sandwich beams with functionally graded rubber core in three point bending, Polym. Compos. 32 (10) (2011) 1541–1551.
[49] M. Yaseer Omar, C. Xiang, N. Gupta, O.M. Strbik, K. Cho, Syntactic foam core metal matrix sandwich composite: compressive properties and strain rate effects, Mater. Sci. Eng.: A 643 (2015) 156–168.
[50] Q.-h. Qin, J.-x. Zhang, Z.-j. Wang, H.-m. Li, D. Guo, Indentation of sandwich beams with metal foam core, Trans. Nonferrous Metals Soc. China 24 (8) (2014) 2440–2446.
[51] A. Rajaneesh, I. Sridhar, S. Rajendran, Relative performance of metal and polymeric foam sandwich plates under low velocity impact, Int. J. Impact Eng. 65 (2014) 126–136.
[52] K. Myers, P. Cortes, B. Conner, T. Wagner, B. Hetzel, K.M. Peters, Structure property relationship of metal matrix syntactic foams manufactured by a binder jet printing process, Addit. Manuf. 5 (2015) 54–59.
[53] I.N. Orbulov, Compressive properties of aluminium matrix syntactic foams, Mater. Sci. Eng.: A 555 (2012) 52–56.
[54] I.N. Orbulov, Metal matrix syntactic foams produced by pressure infiltration—The effect of infiltration parameters, Mater. Sci. Eng.: A 583 (2013) 11–19.
[55] P. Breunig, V. Damodaran, K. Shahapurkar, S. Waddar, M. Doddamani, P. Jeyaraj, P. Prabhakar, Dynamic impact behavior of syntactic foam core sandwich composites, J. Compos. Mater. 54 (4) (2019) 535–547.
[56] S. Waddar, J. Pitchaimani, M. Doddamani, Effect of thermal loading on syntactic foam sandwich composite, Polym. Compos. 41 (5) (2020) 1774–1784.
[57] S. Waddar, J. Pitchaimani, M. Doddamani, E. Barbero, Buckling and vibration behaviour of syntactic foam core sandwich beam with natural fiber composite facings under axial compressive loads, Compos. Part B: Eng. 175 (2019) 107133.
[58] S. Waddar, J. Pitchaimani, M. Doddamani, N. Gupta, Buckling and free vibration behavior of Cenosphere/Epoxy syntactic foams under axial compressive loading, Mater. Perform. Charact. 7 (1) (2018) 532–546.
[59] S. Waddar, J. Pitchaimani, M. Doddamani, Snap-through buckling of fly ash cenosphere/epoxy syntactic foams under thermal environment, Thin-Walled Struct. 131 (2018) 417–427.
[60] S. Waddar, P. Jeyaraj, M. Doddamani, Influence of axial compressive loads on buckling and free vibration response of surface-modified fly ash cenosphere/epoxy syntactic foams, J. Compos. Mater. 52 (19) (2018) 2621–2630.
[61] M. Doddamani, S. Kulkarni, Dynamic response of fly ash reinforced functionally graded rubber composite sandwiches-a Taguchi approach, Int. J. Eng. Sci. Technol. 3 (1) (2011).
[62] A. Petras, Design of Sandwich Structures, University of Cambridge, 1999.
[63] D. Wang, Impact behavior and energy absorption of paper honeycomb sandwich panels, Int. J. Impact Eng. 36 (1) (2009) 110–114.
[64] Y. Yasui, Dynamic axial crushing of multi-layer honeycomb panels and impact tensile behavior of the component members, Int. J. Impact Eng. 24 (6) (2000) 659–671.
[65] R.A.W. Mines, S. Tsopanos, Y. Shen, R. Hasan, S.T. McKown, Drop weight impact behaviour of sandwich panels with metallic micro lattice cores, Int. J. Impact Eng. 60 (2013) 120–132.

[66] H.N.G. Wadley, N.A. Fleck, A.G. Evans, Fabrication and structural performance of periodic cellular metal sandwich structures, Compos. Sci. Technol. 63 (16) (2003) 2331–2343.
[67] S. Park, B.P. Russell, V.S. Deshpande, N.A. Fleck, Dynamic compressive response of composite square honeycombs, Compos. Part A 43 (3) (2012) 527–536.
[68] G.W. Kooistra, D.T. Queheillalt, H.N.G. Wadley, Shear behavior of aluminum lattice truss sandwich panel structures, Mater. Sci. Eng.: A 472 (1) (2008) 242–250.
[69] A.J. Wang, D.L. McDowell, In-plane stiffness and yield strength of periodic metal honeycombs, J. Eng. Mater. Technol. 126 (2) (2004) 137–156.
[70] V. Dikshit, A.P. Nagalingam, G.D. Goh, S. Agarwala, W.Y. Yeong, J. Wei, Quasi-static indentation analysis on three-dimensional printed continuous-fiber sandwich composites, J. Sandw. Struct. Mater. (2019) 1099636219836058, doi:10.1177/1099636219836058.
[71] M.L. Jayavardhan, B.R. Bharath Kumar, M. Doddamani, A.K. Singh, S.E. Zeltmann, N. Gupta, Development of glass microballoon/HDPE syntactic foams by compression molding, Compos. Part B: Eng. 130 (2017) 119–131.
[72] B.R. Bharath Kumar, S.E. Zeltmann, M. Doddamani, N. Gupta, S.Gurupadu Uzma, R.R.N. Sailaja, Effect of cenosphere surface treatment and blending method on the tensile properties of thermoplastic matrix syntactic foams, J. Appl. Polym. Sci. 133 (35) (2016).
[73] B.R.B. Kumar, M. Doddamani, S.E. Zeltmann, N. Gupta, S. Ramakrishna, Data characterizing tensile behavior of cenosphere/HDPE syntactic foam, Data Brief 6 (2016) 933–941.
[74] K. Chockalingam, N. Jawahar, J. Praveen, Enhancement of anisotropic strength of fused deposited ABS parts by genetic algorithm, Mater. Manuf. Processes 31 (15) (2016) 2001–2010.
[75] B.R. Bharath Kumar, M. Doddamani, S.E. Zeltmann, N. Gupta, S. Gurupadu Uzma, R.R.N. Sailaja, Effect of particle surface treatment and blending method on flexural properties of injection-molded cenosphere/HDPE syntactic foams, J. Mater. Sci. 51 (2016) 3793–3805, doi:10.1007/s10853-015-9697-2.
[76] S. Bharath H, Dileep Bonthu, Pavana Prabhakar, M. Doddamani, Three-dimensional printed lightweight composite foams, ACS Omega 5 (35) (2020) 22536–22550.
[77] ISO 22007-2, Plastics — determination of thermal conductivity and thermal diffusivity — Part 2Transient plane Heat Source (hot disc) Method, 2015. International Organization for Standardization ISO Central Secretariat, Chemin de Blandonnet 8 CP 401, 1214 Vernier, Geneva, Switzerland https://www.iso.org/standard/81836.html.